

Breaking the Barriers—Uniting Accelerator and Cosmic Ray p-p Cross Sections

M. M. Block *

*Department of Physics and Astronomy,
Northwestern University, Evanston, IL 60208*

F. Halzen †

*Department of Physics,
University of Wisconsin, Madison, WI 53706*

G. Pancheri

*INFN-Laboratori Nazionali di Frascati,
Frascati, Italy*

T. Stanev‡

Bartol Research Institute, University of Delaware, Newark, DE 19716

Paper presented by Martin M. Block

mblock@nwu.edu

at the

25th Pamir-Chacaltaya Collaboration Workshop, Lodz, Poland, Nov. 3-7, 1999

Abstract

We make a QCD-inspired parameterization of all accelerator data on forward proton-proton and antiproton-proton scattering amplitudes. Using vector dominance and the additive quark model, we show that the same parameters also fit γp and $\gamma\gamma$ interactions. Using the high energy predictions of our model, along with Glauber theory, we calculate proton-air cross sections at energies near $\sqrt{s} \approx 30$ TeV. The comparison of p-air cosmic ray measurements with our QCD model predictions provide a strong constraint on the inclusive particle production cross section.

*Work partially supported by Department of Energy contract DA-AC02-76-Er02289 Task B.

†Work partially supported by Department of Energy contract DE-AC02-76ER0088 and the University of Wisconsin Research Committee with funds granted by the Wisconsin Alumni Research Foundation.

‡Work partially supported by the U.S. Department of Energy under Grant No. DE-FG02-91ER40626.

1 Introduction

This communication is divided into three sections.

First, we show that the data on the total cross section, the slope parameter B of the elastic differential cross section, and the ratio of the real to imaginary part of the forward scattering amplitude ρ for pp and $\bar{p}p$ interactions can be nicely described by a model where high energy cross sections grow with energy as a consequence of the increasing number of soft partons populating the colliding particles [1],[2]. The differential cross sections for the Tevatron and LHC are predicted.

Next, we verify the model by showing that the known experimental data on γp and $\gamma\gamma$ interactions can be derived from our pp and $\bar{p}p$ forward scattering amplitudes using vector meson dominance (VMD) and the additive quark model[2].

Finally, we use the high energy predictions of our QCD-inspired parameterization of accelerator data on forward proton-proton and antiproton-proton scattering amplitudes, along with Glauber theory, to predict proton-air cross sections at energies near $\sqrt{s} \approx 30$ TeV[3].

All cross sections will be computed in an eikonal formalism guaranteeing unitarity throughout:

$$\sigma_{tot}(s) = 2 \int \left\{ 1 - e^{-\chi_I(b,s)} \cos[\chi_R(b,s)] \right\} d^2\vec{b}. \quad (1)$$

Here, χ is the complex eikonal ($\chi = \chi_R + i\chi_I$), and b is the impact parameter. The even eikonal profile function χ^{even} receives contributions from quark-quark, quark-gluon and gluon-gluon interactions, and therefore

$$\begin{aligned} \chi^{even}(s, b) &= \chi_{qq}(s, b) + \chi_{qg}(s, b) + \chi_{gg}(s, b) \\ &= i [\sigma_{qq}(s)W(b; \mu_{qq}) + \sigma_{qg}(s)W(b; \sqrt{\mu_{qq}\mu_{gg}}) + \sigma_{gg}(s)W(b; \mu_{gg})], \end{aligned} \quad (2)$$

where σ_{ij} are the cross sections of the colliding partons, and $W(b; \mu)$ their overlap function in impact parameter space, parameterized as the Fourier transform of a dipole form factor. The impact parameter space distribution function

$$W(b; \mu) = \frac{\mu^2}{96\pi} (\mu b)^3 K_3(\mu b) \quad (3)$$

is normalized so that $\int W(b; \mu) d^2\vec{b} = 1$. As a consequence of both factorization and the normalization chosen for the $W(b; \mu)$, it should be noted that

$$\int \chi^{even}(s, b) d^2\vec{b} = i [\sigma_{gg}(s) + \sigma_{qg}(s) + \sigma_{qq}(s)], \quad (4)$$

so that $\sigma_{tot}^{even}(s) = 2 \text{Im} \{i [\sigma_{gg}(s) + \sigma_{qg}(s) + \sigma_{qq}(s)]\}$, for small χ . This formalism is identical to the one used in “mini-jet” models [4], as well as in simulation programs for minimum-bias hadronic interactions such as PYTHIA and SIBYLL[4].

In this model hadrons asymptotically evolve into black disks of partons. The rising cross section, asymptotically associated with gluon-gluon interactions, is simply parameterized by a normalization, an energy scale, and two parameters: μ_{gg} which describes the “area” occupied by gluons in the colliding hadrons, and $J(= 1 + \epsilon)$. Here, J is defined via the gluonic structure function of the proton, which is assumed to behave as $1/x^J$ for small x . It therefore controls the soft gluon content of the proton. The introduction of the quark-quark and quark-gluon terms allows us to adequately parameterize the data at all energies, since the “size” of quarks and gluons in the proton can be different. In the present context, this model represents a convenient parameterization of the pp and $p\bar{p}$ forward scattering amplitude.

The photoproduction cross sections are calculated from this parameterization assuming vector meson dominance and the additive quark model. For the probability that the photon interacts as a hadron (P_{had}), we use the value $P_{had} = 1/240$ which can be derived from vector meson dominance. Our results show that its value is indeed independent of energy. It is, however, uncertain by 20% because it depends on whether we relate photoproduction to π -nucleon or nucleon-nucleon data (In other words, πN and NN total cross sections only satisfy the additive quark model to this accuracy). Subsequently, following reference [5], we obtain γp cross sections from the assumption that, in the spirit of VMD, the photon is a 2 quark state in

contrast with the proton which is a 3 quark state. The γp total cross section is obtained from the even eikonal for pp and $\bar{p}p$ by the substitutions $\sigma_{ij} \rightarrow \frac{2}{3} \sigma_{ij}$ and $\mu_i \rightarrow \sqrt{\frac{3}{2}} \mu_i$.

We will thus produce a parameter-free description of the total photoproduction cross section, the phase of the forward scattering amplitude and the forward slope for $\gamma p \rightarrow Vp$, where $V = \rho, \omega, \phi$. Interestingly, our results on the phase of $Vp \rightarrow Vp$ are in complete agreement with the values derived from Compton scattering results ($\gamma + p \rightarrow \gamma + p$) using dispersion relations. We also calculate the total elastic and differential cross sections for $\gamma p \rightarrow Vp$. This wealth of data is accommodated without discrepancy.

The $\gamma\gamma$ cross sections are derived following the same procedure. We now substitute $\sigma_{ij} \rightarrow \frac{4}{9} \sigma_{ij}$ and $\mu_i \rightarrow \frac{3}{2} \mu_i$ into the nucleon-nucleon even eikonal, and predict the total cross section and the differential cross sections for all reactions $\gamma\gamma \rightarrow V_i V_j$ at a variety of energies, where $V = \rho, \omega, \phi$.

The high energy $\gamma\gamma$ total cross section [6] have been measured by two experiments at LEP. While these measurements yield new information on its high energy behavior at center-of-mass energies in excess of $\sqrt{s} = 15$ GeV, they may represent the last opportunity to measure the $\gamma\gamma$ cross section, and the two data sets appear to disagree. However, it has been argued that the original data are consistent within the errors [7] and that the observed disagreements are due to two different Monte Carlo's used to extract the quoted values. We here point out that our analysis nicely accommodates the L3 result [8]. Our model approximately satisfies the factorization theorem, $\sigma_{pp}/\sigma_{\gamma p} = \sigma_{\gamma p}/\sigma_{\gamma\gamma}$, because of its small eikonal. The OPAL data do not satisfy it. In fact, no model incorporating the additive quark model and factorization can accommodate the OPAL data. VMD and factorization are sufficient to prevent one from adjusting P_{had} , or any other parameters, to change this conclusion.

2 High energy proton-proton and proton-antiproton scattering

In this section we discuss our QCD-inspired parameterization of the forward amplitudes. To determine its parameters, we fit all high energy forward $\bar{p}p$ and pp scattering data above 15 GeV, for the total cross section (σ_{tot}), the ratio of the real to the imaginary part of the forward scattering amplitude (ρ), and the logarithmic slope of the differential elastic scattering cross section in the forward direction (B). Then, we compare the experimental data for the elastic scattering cross section and for the differential elastic scattering with our results. Finally, a prediction is made for the differential elastic scattering at the LHC.

Our QCD-inspired parameterization satisfies crossing symmetry, *i.e.*, it is either even or odd under the transformation $E \rightarrow -E$, where E is the laboratory energy. This allows us to simultaneously describe $\bar{p}p$ and pp scattering. It also satisfies analyticity, and unitarity because of the eikonal formalism. Since the total cross section asymptotically rises as $\log^2 s$, our QCD-inspired parameterization complies with the Froissart bound. The eikonal formalism for calculating σ_{tot} , ρ and B , along with details on the analyticity, the Froissart bound, and the QCD-inspired eikonal are given in ref. [2]. In all 11 parameters are used. The low energy region, where the differences between $\bar{p}p$ and pp scattering are substantial, largely determines the 7 parameters necessary to fit the odd eikonal and the quark-quark and quark-gluon contribution to the even eikonal. Thus, they largely decouple from the high energy behavior. Hence, for $\sqrt{s} \geq 25$ GeV, where the difference between $\bar{p}p$ and pp scattering becomes small, only 4 parameters describe all data.

We fit all the highest energy cross section data (E710 [9], CDF [10] and the unpublished Tevatron value [11]), which anchor the upper end of our cross section curves. The results of the fit are shown in Fig. 1. Data for ρ values and B are confronted with our model in Figs. 2 and 3.

It can be seen from those figures that we obtain a satisfactory description of all 3 quantities, for both $\bar{p}p$ and pp scattering. The χ^2 of the fit is reasonably good (considering the large spread in some of the experimental data, as well as the discrepancies in the highest energy cross sections), giving a $\chi^2/d.f. = 1.66$, for 75 degrees of freedom. The model splits the difference between the measurements of the total cross section at $\sqrt{s} = 1800$ GeV (see Fig. 1). From Fig. 2, we note that the fit to ρ is anchored at $\sqrt{s} = 550$ GeV by the very accurate measurement [12] of UA4/2 and passes through the E710 point [13]. The statistical uncertainty of the fitted parameters is such that at 25 GeV the cross section predictions are statistically uncertain to $\approx 1.3\%$, at 500 GeV are uncertain to $\approx 1.6\%$, and at 2000 GeV are uncertain to $\approx 2.5\%$.

In Fig. 4 we show the prediction for the elastic cross section along with the data for both $\bar{p}p$ and pp . The agreement is excellent. We note that $\sigma_{elastic}$ is rising more sharply with energy than the total cross section σ_{tot} . Comparing Fig. 1 with Fig. 4, we see that the ratio of the elastic to total cross section is rising with

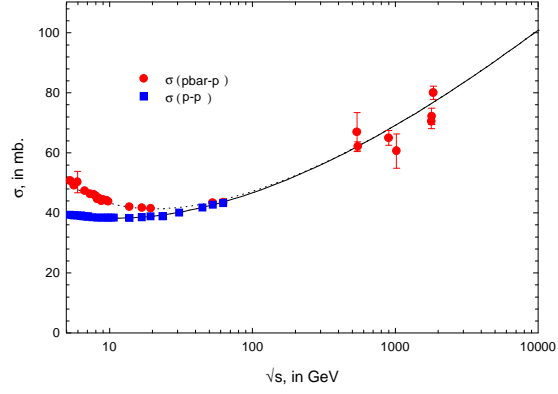


Figure 1: The total cross section for pp and $\bar{p}p$ scattering. The solid line and squares are for pp and the dotted line and circles are for $\bar{p}p$.

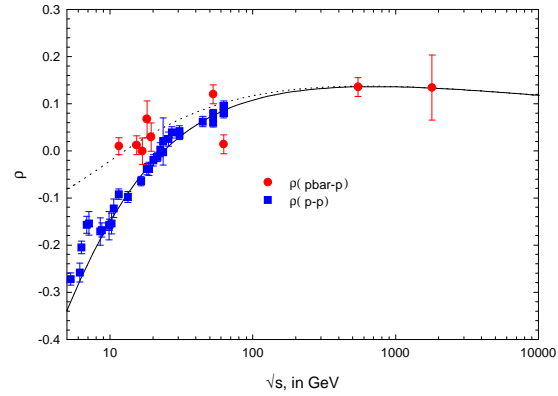


Figure 2: The ratio of the real to imaginary part of the forward scattering amplitude for pp and $\bar{p}p$ scattering. The solid line and squares are for pp and the dotted line and circles are for $\bar{p}p$.

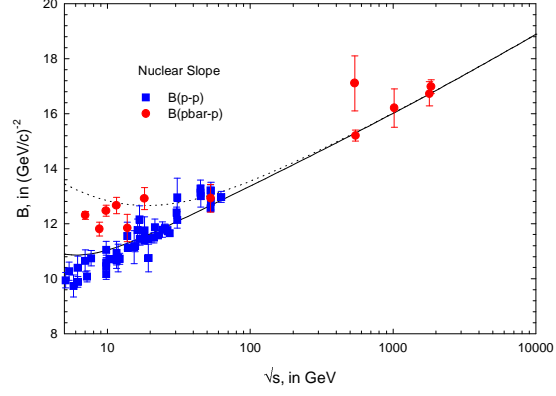


Figure 3: The nuclear slope parameter for elastic pp and $p\bar{p}$ scattering. The solid line and squares are for pp and the dotted line and circles are for $p\bar{p}$.

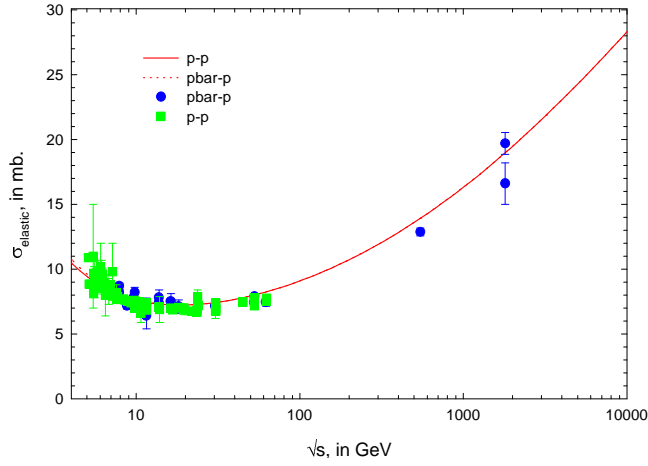


Figure 4: Elastic scattering cross sections for pp and $p\bar{p}$ scattering. The solid line and squares are for pp and the dotted line and circles are for $p\bar{p}$.

energy. The ratio is, of course, bounded by the value for the black disk [14, 15], *i.e.*, 0.5, as the energy goes to infinity.

Having fixed all parameters specifying our eikonal, we calculate $d\sigma/dt$, for various values of \sqrt{s} . The differential cross section at the Tevatron ($\sqrt{s} = 1800$ GeV) is shown in Fig. 5 along with E710 [16] data.

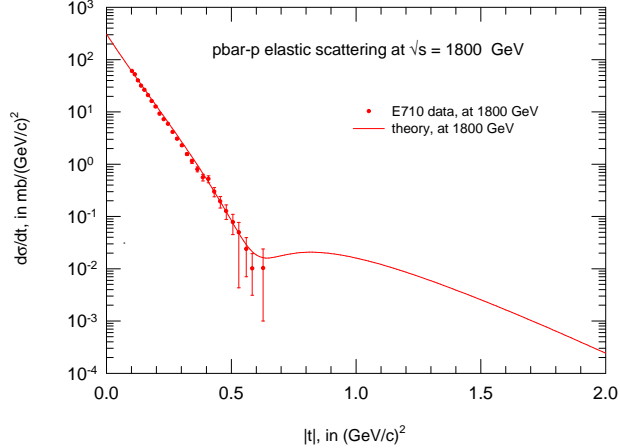


Figure 5: The elastic differential scattering cross section for the reaction $\bar{p}p \rightarrow \bar{p}p$ at $\sqrt{s} = 1800$ GeV. The data points are from E710.

The agreement over 4 decades is striking.

Our prediction for the differential cross section at $\sqrt{s} = 14$ TeV, the energy of the LHC, is plotted in Fig. 6. In particular, at small $|t|$, we predict that the curvature parameter C ($d\sigma/dt \propto e^{Bt+Ct^2}$ for small t ;

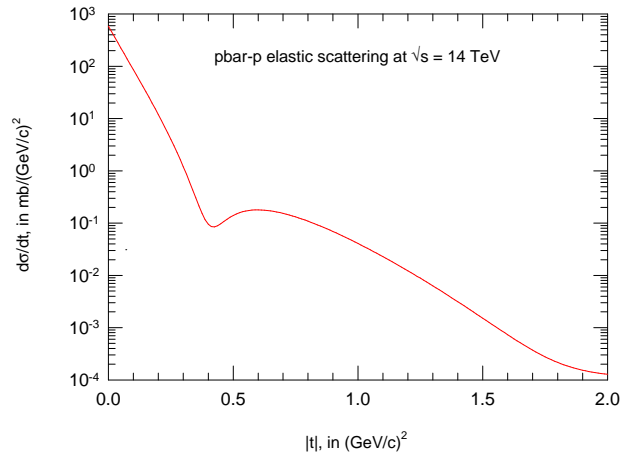


Figure 6: The elastic differential scattering cross section for the reaction $\bar{p}p \rightarrow \bar{p}p$ at LHC.

see ref. [14] for details) is negative. For energies much lower than 1800 GeV, the observed curvature has been measured as positive. For 1800 GeV, we see from Fig. 5 that the curvature parameter C is compatible with being zero. Block and Cahn [14, 15] have pointed out that the curvature is predicted to go through zero near the Tevatron energy and that it should become negative thereafter. Asymptotically the proton approaches a black disk. Its curvature is always negative [14, 15], $C = -R^4/192$, where R is the radius of

the disk. Thus, the curvature has to pass through zero as the energy increases. ‘Asymptopia’ is the energy region (energies much larger than the Tevatron) where the scattering approaches that of a sharp disk.

With the parameters we obtained from our fit, the total cross section at the LHC (14 TeV) is predicted to be $\sigma_{tot} = 108.0 \pm 3.4$ mb, where the error is due to the statistical errors of the fitting parameters.

3 Photon-proton reactions

We assume that the photon behaves like a two quark system when it interacts strongly. We therefore obtain γp scattering amplitudes by performing the substitutions $\sigma_{ij} \rightarrow \frac{2}{3}\sigma_{ij}$ and $\mu_i \rightarrow \sqrt{\frac{3}{2}}\mu_i$ in the even eikonal for nucleon–nucleon scattering, so that

$$\chi^{\gamma p}(s, b) = i \left[\frac{2}{3}\sigma_{qq}(s)W\left(b; \sqrt{\frac{3}{2}}\mu_{qq}\right) + \frac{2}{3}\sigma_{qg}(s)W\left(b; \sqrt{\frac{3}{2}}\mu_{qq}\mu_{gg}\right) + \frac{2}{3}\sigma_{gg}(s)W\left(b; \sqrt{\frac{3}{2}}\mu_{gg}\right) \right]. \quad (5)$$

Using vector dominance, the photon-proton total cross section is then written as

$$\sigma_{tot}^{\gamma p}(s) = 2P_{had} \int \left\{ 1 - e^{-\chi_I^{\gamma p}(b, s)} \cos[\chi_R^{\gamma p}(b, s)] \right\} d^2\vec{b}, \quad (6)$$

where P_{had} is the probability that a photon interacts as a hadron. We use the value $P_{had} = 1/240$. This value is found by normalizing the total γp cross section to the low energy data, and is very close to that derived from vector dominance, $1/249$. Using $f_\rho^2/4\pi = 2.2$, $f_\omega^2/4\pi = 23.6$ and $f_\phi^2/4\pi = 18.4$, we find $\Sigma_V(4\pi\alpha/f_V^2) = 1/249$, where $V = \rho, \omega, \phi$ (see Table XXXV, pag. 393 of Ref. [17]).

With all eikonal parameters fixed by the nucleon-nucleon data, we can now calculate $\sigma_{tot}^{\gamma p}(s)$. The result is shown in Fig. 7. It reproduces the rising cross section for γp , using the parameters fixed by nucleon-nucleon

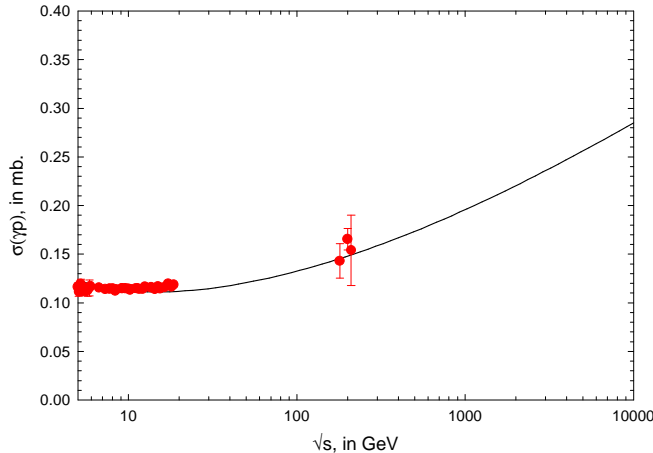


Figure 7: The total cross section for γp scattering.

scattering. This prediction only uses the 9 parameters of the even eikonal, of which but 4 are important in the upper energy region. The accuracy of our predictions are $\sim 1.5\%$, from the statistical uncertainty in our eikonal parameters.

We next consider the ‘elastic’ scatterings

$$\begin{aligned} \gamma + p &\rightarrow \rho_{virtual} + p \rightarrow \rho + p, \\ \gamma + p &\rightarrow \omega_{virtual} + p \rightarrow \omega + p, \\ \gamma + p &\rightarrow \phi_{virtual} + p \rightarrow \phi + p. \end{aligned} \quad (7)$$

Here the photon virtually transforms into a vector meson which elastically scatters off of the proton. The strengths of these reactions is $\mathcal{O}(\alpha)$ times a strong interaction cross section. The true elastic cross section is

given by Compton scattering on the proton, $\gamma + p \rightarrow \gamma + p$, which we can visualize as

$$\begin{aligned}\gamma + p &\rightarrow \rho_{\text{virtual}} + p \rightarrow \rho + p \rightarrow \gamma + p, \\ \gamma + p &\rightarrow \omega_{\text{virtual}} + p \rightarrow \omega + p \rightarrow \gamma + p, \\ \gamma + p &\rightarrow \phi_{\text{virtual}} + p \rightarrow \phi + p \rightarrow \gamma + p.\end{aligned}\tag{8}$$

It is clearly $\mathcal{O}(\alpha^2)$ times a strong interaction cross section, and hence is much smaller than ‘elastic’ scattering of Eq. (7). Thus, we justify the use of Eq. (6) to calculate the total cross section, since only reactions with a photon in the final state are neglected.

We evaluate ρ and the slope B for the ‘elastic’ scattering expressed in Eq. (7), with ρ and B being the same for all 3 reactions.

The dependence of ρ with the energy is shown in Fig. 8. Damashek and Gilman [18] have calculated the ρ value for Compton scattering on the proton using dispersion relations, *i.e.*, the true elastic scattering reaction for photon-proton scattering. We compare this calculation, the dotted line in Fig. 8, with our

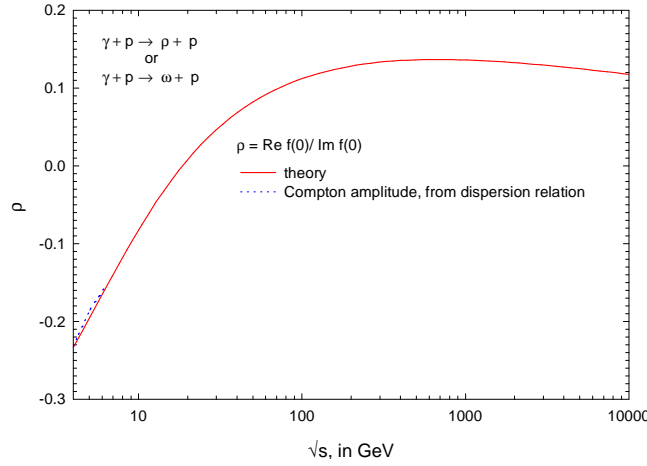


Figure 8: Ratio of the real to imaginary part of the forward scattering amplitude for the ‘elastic’ reactions $\gamma + p \rightarrow V_i + p$, where V_i is ρ^0 , ω^0 or ϕ^0 . The dotted curve is for Compton scattering from dispersion relations [18]. It has been slightly displaced from the solid curve for clarity in viewing.

prediction of ρ (the solid line). The agreement is so close that we had to move the two curves apart so that they may be viewed more clearly.

In Fig. 9 we show our results for the slope B as a function of the energy. The available experimental data for ‘elastic’ ρp and ωp final states are also plotted. Again, the agreement of theory and experiment is very good.

To calculate the elastic cross sections $\sigma_{\text{elastic}}^{Vp}$ and differential cross sections $d\sigma^{Vp}/dt$ as a function of energy, we use

$$\sigma_{\text{elastic}}^{Vp}(s) = P_{\text{had}}^{Vp} \int \left| 1 - e^{i\chi^{\gamma p}(b,s)} \right|^2 d^2\vec{b},\tag{9}$$

where P_{had}^{Vp} is the appropriate probability for a photon to turn into V , with $V = \rho, \omega$ or ϕ . The differential scattering cross section is given by

$$\frac{d\sigma^{Vp}}{dt}(s,t) = \frac{P_{\text{had}}^{Vp}}{4\pi} \left| \int J_0(qb)(1 - e^{i\chi^{\gamma p}(b,s)}) d^2\vec{b} \right|^2,\tag{10}$$

where $t = -q^2$.

Since we normalize our data to the cross section found with $\chi^{\gamma p}$, and not to $(\sigma_{\text{tot}}^+ + \sigma_{\text{tot}}^-)/2$, we must multiply all $f_V^2/4\pi$ by 1.65. Hence, our effective couplings are $f_{\rho\text{eff}}^2/4\pi = 3.6$, $f_{\omega\text{eff}}^2/4\pi = 38.9$, and $f_{\phi\text{eff}}^2/4\pi = 30.4$.

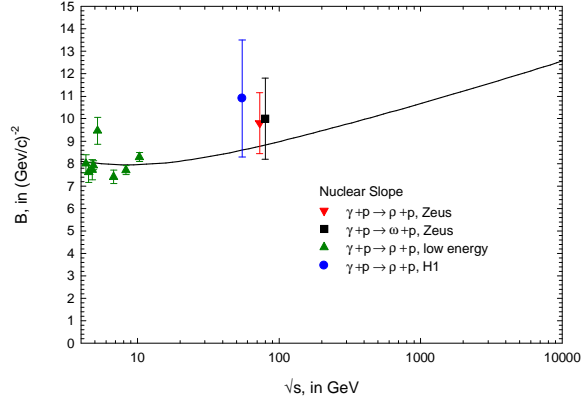


Figure 9: Nuclear slope parameter for the ‘elastic’ reaction $\gamma + p \rightarrow V_i + p$, where V_i is ρ^0 , ω^0 or ϕ . For the reaction $\gamma + p \rightarrow \rho^0 + p$, the inverted triangles are the Zeus data, the circles are the H1 data, and the triangles are the low energy data. For the reaction $\gamma + p \rightarrow \omega^0 + p$, the squares are the Zeus data.

Our evaluation of the ‘elastic’ cross section for the reactions $\gamma + p \rightarrow \rho^0 + p$ and $\gamma + p \rightarrow \omega^0 + p$ are shown in Figs. 10 and 11, respectively.

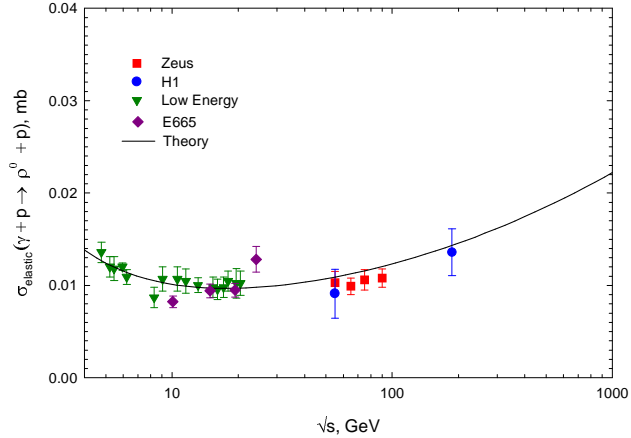


Figure 10: The ‘elastic’ photoproduction cross section, for the reaction $\gamma + p \rightarrow \rho^0 + p$. The squares are Zeus data, the circles are H1 data, and the inverted triangles the low energy data.

The differential cross section, $d\sigma/dt$, for the ‘elastic’ reactions $\gamma + p \rightarrow \rho^0 + p$, $\gamma + p \rightarrow \omega^0 + p$ and $\gamma + p \rightarrow \phi^0 + p$ are plotted in Figs. 12, 13, and 14, respectively. The agreement, in absolute normalization and shape, of our results for all three light vector mesons with the experimental data for all available energies reinforces our confidence in the model.

4 Photon-Photon Interactions

In this section, we consider $\gamma\gamma$ interactions. As it was done for γp interactions, we will start from the eikonal $\chi^{\gamma p}(s, b)$ and multiply every cross section by $2/3$ and multiply each μ by $\sqrt{3/2}$. Therefore,

$$\chi^{\gamma\gamma}(s, b) = i \left[\frac{4}{9} \sigma_{qq}(s) W \left(b; \frac{3}{2} \mu_{qq} \right) + \frac{4}{9} \sigma_{qg}(s) W \left(b; \frac{3}{2} \sqrt{\mu_{qq} \mu_{gg}} \right) + \frac{4}{9} \sigma_{gg}(s) W \left(b; \frac{3}{2} \mu_{gg} \right) \right]. \quad (11)$$

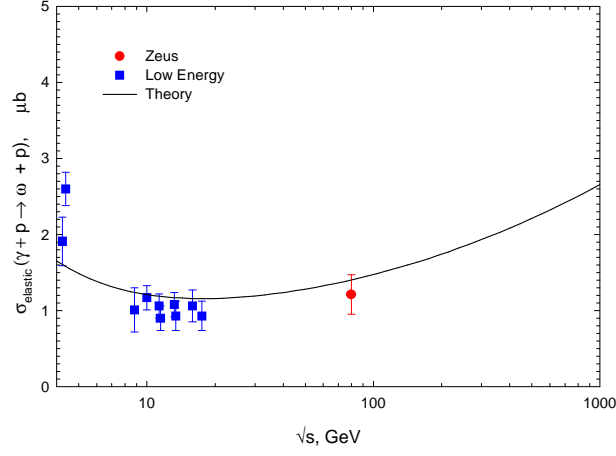


Figure 11: The ‘elastic’ photoproduction cross section for the reaction $\gamma + p \rightarrow \omega^0 + p$. The circles are Zeus data, and the squares are the low energy data.

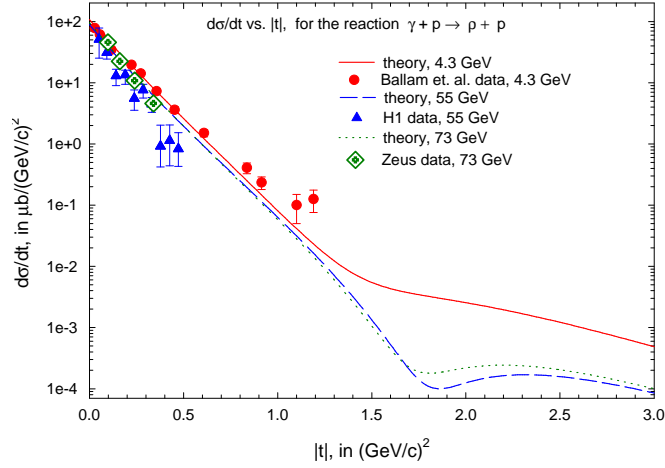


Figure 12: The differential cross section for the ‘elastic’ reaction $\gamma + p \rightarrow \rho^0 + p$. The solid curve and the circles (Ballam *et al.* data) are at $\sqrt{s} = 4.3$ GeV, the dashed curve and triangles (H1 data) are at $\sqrt{s} = 55$ GeV, and the dotted curve and diamonds are at $\sqrt{s} = 73$ GeV (Zeus data).

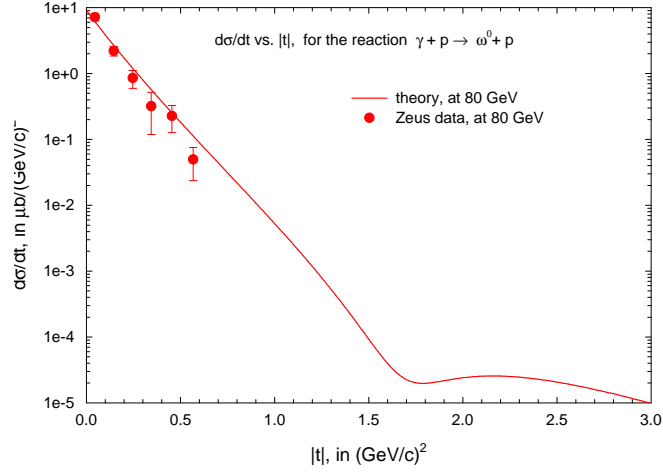


Figure 13: The differential cross section for the ‘elastic’ reaction $\gamma + p \rightarrow \omega^0 + p$ at $\sqrt{s}=80$ GeV. The circles are the Zeus data.

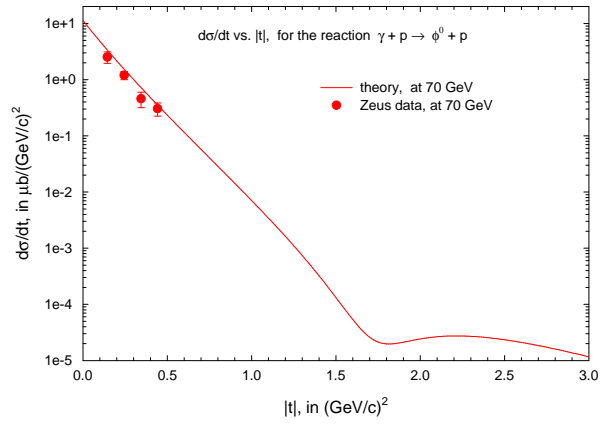


Figure 14: The differential cross section for the ‘elastic’ reaction $\gamma + p \rightarrow \phi^0 + p$ at $\sqrt{s}=70$ GeV. The circles are the Zeus data.

Using vector dominance we obtain,

$$\sigma_{tot}^{\gamma\gamma}(s) = 2P_{had}^2 \int \left\{ 1 - e^{-\chi_I^{\gamma\gamma}(b,s)} \cos[\chi_R^{\gamma\gamma}(b,s)] \right\} d^2\vec{b}, \quad (12)$$

where $P_{had} = 1/240$ is the probability that a photon will interact as a hadron. In Fig. 15 we plot our results

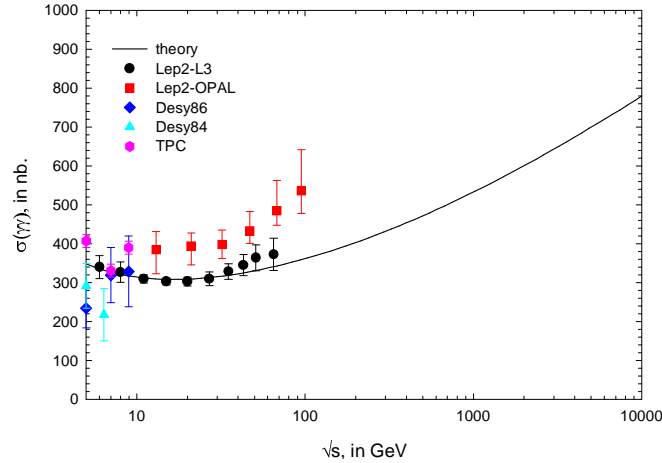


Figure 15: The total cross section for $\gamma\gamma$ scattering. The data sources are indicated in the legend.

for $\sigma_{tot}^{\gamma\gamma}(s)$ as a function of the energy, and compare it to the various sets of experimental data. We note that our prediction fits the L3 data, but doesn't fit the OPAL results.

5 Proton-air cross sections

Cosmic ray experiments measure the penetration in the atmosphere of particles with energies in excess of those accelerated by existing machines—interestingly, their energy range covers the energy of the Large Hadron Collider (LHC) and extends beyond it. However, extracting proton-proton cross sections from cosmic ray observations is far from straightforward [19]. By a variety of experimental techniques, cosmic ray experiments map the atmospheric depth at which cosmic ray initiated showers develop. The measured shower attenuation length (Λ_m) is not only sensitive to the interaction length of the protons in the atmosphere (λ_{p-air}), with

$$\Lambda_m = k\lambda_{p-air} = k \frac{13.5m_p}{\sigma_{p-air}^{inel}}, \quad (13)$$

but also depends on the rate at which the energy of the primary proton is dissipated into electromagnetic shower energy observed in the experiment. The latter effect is parameterized in Eq. (13) by the parameter k ; m_p is the proton mass and σ_{p-air}^{inel} the inelastic proton-air cross section. The value of k depends on the inclusive particle production cross section in nucleon and meson interactions on the light nuclear target of the atmosphere and its energy dependence. We here ignored the fact that particles in the cosmic ray "beam" may be nuclei, not just protons. Experiments allow for this by omitting from their analysis showers which dissipate their energy high in the atmosphere, a signature that the initial energy is distributed over the constituents of a nucleus.

The extraction of the pp cross section from the cosmic ray data is a two step process. First, one calculates the p -air total cross section from the measured inelastic cross section

$$\sigma_{p-air}^{inel} = \sigma_{p-air} - \sigma_{p-air}^{el} - \sigma_{p-air}^{q-el}. \quad (14)$$

Next, the Glauber method[20] is used to transform the measured value of σ_{p-air}^{inel} into a proton-proton total cross section σ_{pp} ; all the necessary steps are calculable in the theory. In Eq. (14) the measured cross section

for particle production is supplemented with the elastic and quasi-elastic cross section, as calculated by the Glauber theory, to obtain the total cross section $\sigma_{p\text{-air}}$. The subsequent relation between $\sigma_{p\text{-air}}^{\text{inel}}$ and σ_{pp} involves the slope of the forward scattering amplitude for elastic pp scattering,

$$B = \left[\frac{d}{dt} \left(\ln \frac{d\sigma_{pp}^{\text{el}}}{dt} \right) \right]_{t=0}, \quad (15)$$

and is shown in Fig. 16, which plots B against σ_{pp} , for 5 curves of different values of $\sigma_{p\text{-air}}^{\text{inel}}$. This summarizes

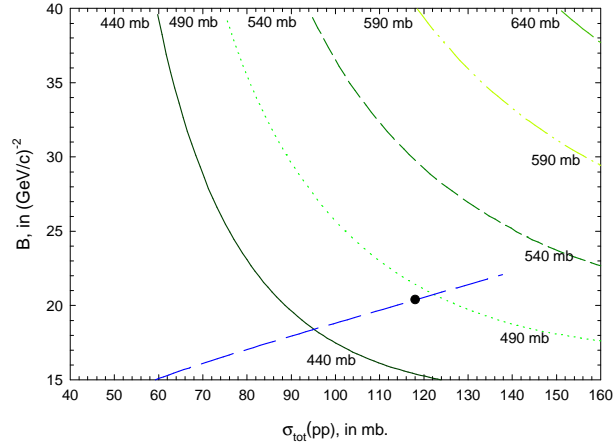


Figure 16: B dependence on the pp total cross section σ_{pp} . The five curves are lines of constant $\sigma_{p\text{-air}}^{\text{inel}}$, of 440, 490, 540, 590 and 640 mb—the central value is the published Fly’s Eye value, and the others are $\pm 1\sigma$ and $\pm 2\sigma$. The dashed curve is a plot of our QCD-inspired fit of B against σ_{pp} . The dot is our value for $\sqrt{s} = 30$ TeV, the Fly’s Eye energy.

the reduction procedure from $\sigma_{p\text{-air}}^{\text{inel}}$ to σ_{pp} [19]. Also plotted in Fig. 16 is a curve of B vs. σ_{pp} which will be discussed later.

A significant drawback of the method is that one needs a model of proton–air interactions to complete the loop between the measured attenuation length Λ_m and the cross section $\sigma_{p\text{-air}}^{\text{inel}}$, *i.e.*, the value of k in Eq. (13). We minimize the impact of theory by using our QCD-inspired parameterization of the forward proton–proton and proton–antiproton scattering amplitudes which is analytic, unitary and *simultaneously* fits all data of σ_{tot} , B and ρ . Using vector meson dominance and the additive quark models, we have shown that it accommodates a wealth of data on photon–proton and photon–photon interactions without the introduction of new parameters. Because the model is both unitary and analytic, it has high energy predictions that are essentially theory–independent. In particular, it also *simultaneously* fits σ_{pp} and B , forcing a relationship between the two. Specifically, the B vs. σ_{pp} prediction of the model is shown as the dashed curve in Fig. 16. The dot corresponds to our prediction of σ_{pp} and B at $\sqrt{s} = 30$ TeV. It is seen to be slightly below the curve for 490 mb, the lower limit of the Fly’s Eye measurement, which was made at $\sqrt{s} \approx 30$ TeV.

In Fig. 17, we have plotted the values of σ_{pp} vs. $\sigma_{p\text{-air}}^{\text{inel}}$ that are deduced from the intersections of the B – σ_{pp} curve with the $\sigma_{p\text{-air}}^{\text{inel}}$ curves of Fig. 16. Figure 17 allows the conversion of the measured $\sigma_{p\text{-air}}^{\text{inel}}$ to σ_{pp} .

Our prediction for the total cross section σ_{pp} as a function of energy is confronted with all of the accelerator and cosmic ray measurements[21, 22, 23] in Fig. 18. For inclusion in Fig. 18, we have calculated the cosmic ray values of σ_{pp} from the *published* experimental values of $\sigma_{p\text{-air}}^{\text{inel}}$, using the results of Fig. 17. We note the predicted curve is systematically lower than the cosmic ray points, roughly about the level of one standard deviation.

It is at this point important to recall Eq. (13) and consider the fact that the extraction of $\sigma_{p\text{-air}}^{\text{inel}}$ from the measurement of Λ_m requires a determination of the parameter k . The measured depth X_{max} at which a shower reaches maximum development in the atmosphere, which is the basis of the cross section measurement

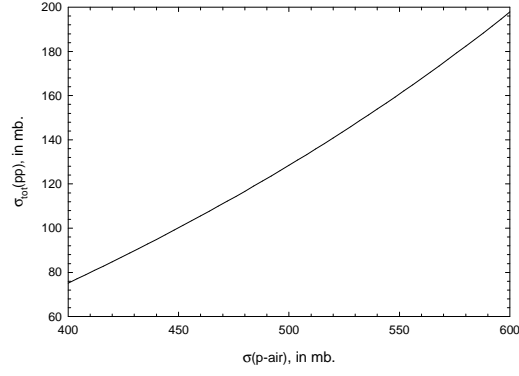


Figure 17: A plot of the predicted total pp cross section σ_{pp} , in mb *vs.* the measured p-air cross section, $\sigma_{p\text{-air}}^{\text{inel}}$, in mb.

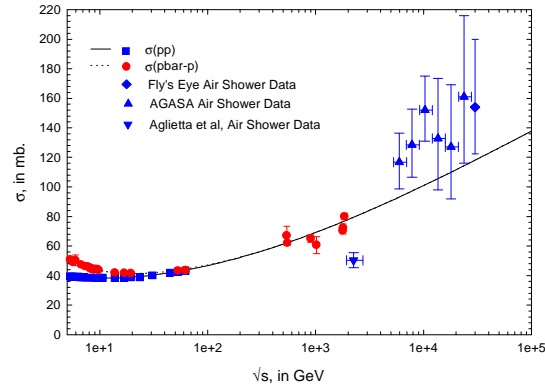


Figure 18: A plot of the QCD-inspired fit of the total nucleon-nucleon cross section σ_{pp} , in mb *vs.* \sqrt{s} , in GeV. The cosmic ray data that are shown have been converted from $\sigma_{p\text{-air}}^{\text{inel}}$ to σ_{pp} using the results of Fig. 17.

in Ref. [21], is a combined measure of the depth of the first interaction, which is determined by the inelastic cross section, and of the subsequent shower development, which has to be corrected for. The position of X_{\max} also directly affects the rate of shower attenuation with atmospheric depth which is the alternative procedure for extracting $\sigma_{p\text{-air}}^{\text{inel}}$.

The model dependent rate of shower development and its fluctuations are the origin of the deviation of k from unity in Eq. (13). Its values range from 1.5 for a model where the inclusive cross section exhibits Feynman scaling, to 1.1 for models with large scaling violations[19]. The comparison between data and experiment in Fig. 18 is further confused by the fact that the AGASA[22] and Fly's Eye[21] experiments used different values of k in the analysis of their data, *i.e.*, AGASA used $k = 1.5$ and Fly's Eye used $k = 1.6$.

We therefore decided to match the data to our prediction and extracted a common value for $k = 1.33 \pm 0.04$. This neglects the possibility that k may show a weak energy dependence over the range measured. In Fig. 19 we have replotted the high energy cosmic ray data for our prediction of $\sigma_{p\text{-air}}^{\text{inel}}$ *vs.* \sqrt{s} , with the

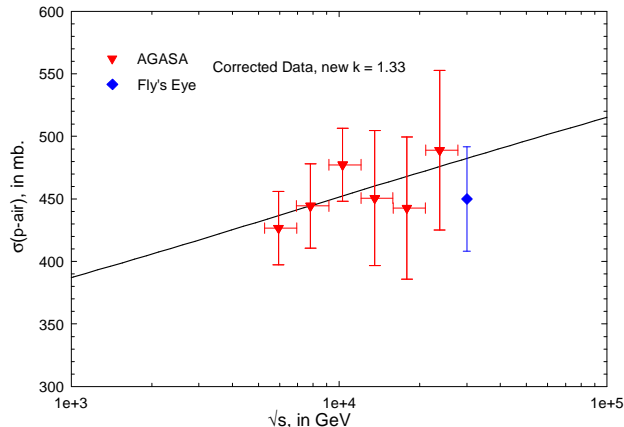


Figure 19: A χ^2 fit of the measured AGASA and Fly's Eye data for $\sigma_{p\text{-air}}^{\text{inel}}$, in mb, as a function of the energy, \sqrt{s} , in GeV. The result of the fit for the parameter k in Eq. (13) is $k = 1.33 \pm 0.04$.

common value of 1.33 obtained from a χ^2 fit. Clearly, we have an excellent fit, with good agreement between AGASA and Fly's Eye. The analysis gives $\chi^2 = 1.75$ for 6 degrees of freedom (the low χ^2 is probably due to overestimates of experimental errors). This result for k is interesting—it is close to the value of 1.2 obtained using the SIBYLL simulation[24] for inclusive particle production. This represents a consistency check in the sense that our model for forward scattering amplitudes and SIBYLL share the same underlying physics. The increase of the total cross section with energy to a black disk of soft partons is the shadow of increased particle production which is modeled by the production of (mini)-jets in QCD. The difference between the k values of 1.20 and 1.33 could be understood because the experimental measurement integrates showers in a relatively wide energy range, which tends to increase the value of k .

In the near term, we look forward to the possibility of repeating this analysis with the higher statistics of the HiRes [25] cosmic ray experiment that is currently in progress and the Auger [26] Observatory.

In conclusion, we have successfully united the high energy cross section results ($\sqrt{s} \approx 30$ TeV) of the cosmic ray measurements with the accelerator cross section measurements, under a common rubric, the QCD-inspired analysis.

References

- [1] M. M. Block, R. Fletcher, F. Halzen, B. Margolis, and P. Valin, Phys. Rev. D **41**, 978 (1990).
- [2] M. M. Block, E. M. Gregores, F. Halzen, and G. Pancheri, Phys. Rev. D **60**, 054024 (1999).
- [3] M. M. Block, Francis Halzen, and Todor Stanev, hep-ph/9908222; Phys. Rev. Lett. **83**, 4926 (1999).

- [4] D. Cline, F. Halzen, and J. Luthe, Phys. Rev. Lett. **31**, 491 (1973); P. l'Hereux, B. Margolis, and P. Valin, Phys. Rev. D **32**, 1681 (1985); L. Durand and H. Pi, Phys. Rev. Lett. **58**, 303 (1987); Phys. Rev. D **40**, 1436 (1989); V. Innocente, A. Capella, and J. T. T. Van, Phys. Lett. B **213**, 81 (1988); B. Margolis *et al.*, Phys. Lett. B **213**, 221 (1988); B. Z. Kopeliovich, N. N. Nikolaev, and I. K. Potashnikova, Phys. Rev. D **39**, 769 (1989); T. K. Gaisser and T. Stanev, Phys. Lett. B **219**, 375 (1989); J. C. Collins and G. A. Ladinsky, Phys. Rev. D **43**, 2847 (1991).
- [5] R. S. Fletcher, T. K. Gaisser, and F. Halzen, Phys. Rev. D **45**, 377 (1992); Phys. Rev. D **45**, 3279 (1992) (E); Phys. Lett. B **298**, 442 (1993).
- [6] PLUTO Collaboration, Ch. Berger *et al.*, Phys. Lett. B **149**, 421 (1984); TPC/ 2γ Collaboration, H. Aihara *et al.*, Phys. Rev. D **41**, 2667 (1990); MD-1 Collaboration, S. E. Baru *et al.*, Z. Phys. C **53**, 219 (1992); L3 Collaboration, M. Acciarri *et al.*, Phys. Lett. B **408**, 450 (1997); F. Wackerle, Nucl. Phys. Proc. Suppl. **71**, 381 (1999).
- [7] S. Soldner-Rembold, hep-ex/9810011, proceedings of the *ICHEP'98*, Vancouver, July 1998.
- [8] M. M. Block, E. M. Gregores, F. Halzen, and G. Pancheri, Phys. Rev. D **58**, 017503 (1998).
- [9] E710 Collaboration, N. Amos *et al.*, Phys. Rev. Lett. **63**, 2784 (1989).
- [10] CDF Collaboration, F. Abe *et al.*, Phys. Rev. D **50**, 5550 (1994).
- [11] J. Orear, proceedings of the *International Conference (7th Blois Workshop) on Elastic and Diffractive Scattering—Recent Advances in Hadron Physics*, Seoul, Korea, June 1997.
- [12] UA4 Collaboration, C. Augier *et al.*, Phys. Lett. B **316**, 448 (1993).
- [13] E710 Collaboration, N. Amos *et al.*, Phys. Rev. Lett. **68**, 2433 (1992).
- [14] M. M. Block and R. N. Cahn, Rev. Mod. Phys. **57**, 563 (1985).
- [15] M. M. Block, R. N. Cahn, Phys. Lett. B **149**, (1984).
- [16] E710 Collaboration, N. Amos *et al.*, Phys. Rev. Lett. **61**, 525 (1988).
- [17] T. H. Bauer *et al.*, Rev. Mod. Phys. **50**, 261 (1978).
- [18] M. Damashek and F. J. Gilman, Phys. Rev. D **1**, 1319 (1970).
- [19] R. Engel *et al.*, Phys. Rev. D **58** 014019, 1998.
- [20] T. K. Gaisser *et al.*, Phys. Rev. D **36**, 1350, 1987.
- [21] R. M. Baltrusaitis *et al.*, Phys. Rev. Lett. **52**, 1380, 1984.
- [22] M. Honda *et al.*, Phys. Rev. Lett. **70**, 525, 1993.
- [23] M. Aglietta *et al.*, Proc 25th ICRC (Durban) **6**, 37, 1997.
- [24] R. S. Fletcher *et al.*, Phys. Rev. D **50**, 5710, 1994.
- [25] See <http://sunshine.chpc.utah.edu/research/cosmic/hires/>
- [26] The Pierre Auger Project Design Report, Fermilab report (Feb. 1997).